

Data-Driven Convex Approach to Off-road Navigation via Linear Transfer Operators

Joseph Moyalan, Yongxin Chen and Umesh Vaidya

Abstract—We consider the problem of optimal navigation control design for navigation on off-road terrain. We use traversability measure to characterize the degree of difficulty of navigation on the off-road terrain. The traversability measure captures the property of terrain essential for navigation, such as elevation map, terrain roughness, slope, and terrain texture. The terrain with the presence or absence of obstacles becomes a particular case of the proposed traversability measure. We provide a convex formulation to the off-road navigation problem by lifting the problem to the density space using the linear Perron-Frobenius (P-F) operator. The convex formulation leads to an infinite-dimensional optimal navigation problem for control synthesis. The finite-dimensional approximation of the infinite-dimensional convex problem is constructed using data. We use a computational framework involving the Koopman operator and the duality between the Koopman and P-F operator for the data-driven approximation. This makes our proposed approach data-driven and can be applied in cases where an explicit system model is unavailable. Finally, we demonstrate the application of the developed framework for the navigation of vehicle dynamics with Dubin’s car model.

I. INTRODUCTION

The navigation problem is extensively studied in the robotics community. More recently, the problem of off-road navigation has received more interest and is driven by robotics applications in an unstructured environment. The objective is to drive a robot/vehicle from some initial set to reach the desired target set through an obstacle-ridden environment. One of the popular approaches to navigation is the use of navigation functions. Controller derived using navigation functions relies on the negative gradient of the function to drive the system to the target set. However, due to the nonconvex nature of the navigation function, the gradient-based controller gets stuck in the local minimum [1], [2]. Unlike classical navigation problems where the obstacles are binary, i.e., either there is an obstacle or no obstacle, the entire region can be riddled with obstacles with varying degrees of difficulty for off-road navigation. The control design of such navigation problems is based on geometric mapping of the unstructured environment through the use of sensors on the mobile robot such as LIDAR and cameras [3]–[5]. The control design of such navigation problems often leads to a nonconvex formulation. Hence providing guarantees for global

optimality remains a challenge. Research involving vision-based off-road navigation have also gained prominence [6]–[8]. However, since the underlying formulation relies on solving a nonconvex optimization problem, the vision-based approaches lack a systematic structure.

In this paper, we explore the traversability description of the terrain, i.e., the level of difficulty in navigating using a traversability measure. The terrain’s traversability measure depends on the terrain parameters such as elevation map, terrain roughness, slope, and terrain texture. In this paper, we have utilized the normalized elevation map while constructing the traversability measure. The traversability measure is used to assign a varying degree of difficulty to pass through a given region in the terrain based on the value of the traversability measure on the region. The larger the value of traversability measure on a region, the more difficult it is to navigate through that region. In addition to this, the traversability measure of a smooth terrain with binary obstacles will be a particular case of the proposed approach.

We consider the problem of data-driven navigation control design while considering the traversability constraints. The data-driven element of the framework makes it possible to work in situations where explicit dynamics of the vehicle model are not available. For an unmanned ground vehicle (UGV), this data comes from the wheel odometry, and GPS/IMU sensor [4], [9], [10]. The main contribution of this paper is in providing a convex formulation to the optimal navigation problem in off-road terrain. Furthermore, we show how the traversability measure can be used to design a meaningful cost function suitable for off-road navigation. The convex formulation is made possible by lifting the navigation problem in the space of density using methods from linear operator theory involving Perron-Frobenius operator. The convex formulation is inspired from the work in [11] for optimal control problems and later exploited for navigation with deterministic and stochastic obstacles in [12]–[15]. The incorporation of the traversability measure and density-based formulation for off-road navigation is novel to this paper. The convex formulation leads to an infinite-dimensional convex optimization problem for off-road navigation. The finite-dimensional approximation of the infinite-dimensional convex problem is constructed using data. We use a computational framework involving the Koopman operator and the duality between the Koopman and P-F operator for the data-driven approximation. Compared

Financial support from NSF under grants 1942523, 2008513, 2031573 and NSF CPS award 1932458 is greatly acknowledged. J. Moyalan and U. Vaidya are with the Department of Mechanical Engineering, Clemson University, Clemson, SC; {jmoyala,uvaidya}@clemson.edu. Y. Chen is with the School of Aerospace Engineering, Georgia Institute of Technology, Atlanta, GA; {yongchen}@gatech.edu

to our earlier work [11], the data-driven computation framework proposed in this paper is numerically efficient. Finally, we demonstrate the application of the developed framework for off-road navigation of vehicle dynamics with the Dubin car model.

The rest of the paper is structured as follows. Section II provides a brief introduction to our framework's necessary preliminaries. Section III consists of problem formulation and the main results are discussed in Section IV. In Section V, we develop the computational framework based on the linear operator framework. Simulation results are presented in Section VI and a conclusion in Section VII.

II. BACKGROUND AND NOTATIONS

Consider the dynamical system

$$\dot{\mathbf{x}} = \mathbf{F}(\mathbf{x}), \quad \mathbf{x} \in \mathbf{X} \subseteq \mathbb{R}^n \quad (1)$$

where it is assumed that $\mathbf{F}(\mathbf{x}) \in \mathcal{C}^1(\mathbf{X}, \mathbb{R}^n)$, i.e. the space of continuously differentiable functions on \mathbf{X} . Let us denote $\mathbf{s}_t(\mathbf{x})$ to be the solution of dynamical system (1) at time t . $\mathcal{B}(\mathbf{X})$ denotes the Borel σ -algebra on \mathbf{X} and $\mathcal{M}(\mathbf{X})$ is the vector space of real-valued measure on $\mathcal{B}(\mathbf{X})$. Also note that, $\mathcal{L}_\infty(\mathbf{X})$ and $\mathcal{L}_1(\mathbf{X})$ represents the space of essentially bounded and integrable functions on \mathbf{X} respectively. The lifting of the finite dimensional nonlinear dynamics from state space to infinite dimension space of functions may be done in two different ways namely using Koopman and Perron-Frobenius operators [16].

Definition II.1 (Koopman Operator). \mathbb{U}_t for dynamical system (1) is defined as

$$[\mathbb{U}_t\phi](\mathbf{x}) = \phi(\mathbf{s}_t(\mathbf{x})), \quad (2)$$

where ϕ is a test function in the lifted function space $\mathcal{L}_\infty(\mathbf{X}) \cap \mathcal{C}^1(\mathbf{X})$. The infinitesimal generator for the Koopman operator is given by

$$\lim_{t \rightarrow 0} \frac{[\mathbb{U}_t\phi](\mathbf{x}) - \phi(\mathbf{x})}{t} = \mathbf{F}(\mathbf{x}) \cdot \nabla\phi(\mathbf{x}) =: \mathcal{U}_{\mathbf{F}}\phi. \quad (3)$$

Definition II.2 (Perron-Frobenius Operator). $\mathbb{P}_t : \mathcal{L}_1(\mathbf{X}) \rightarrow \mathcal{L}_1(\mathbf{X})$ for dynamical system (1) is defined as

$$[\mathbb{P}_t\varphi](\mathbf{x}) = \varphi(\mathbf{s}_{-t}(\mathbf{x})) \left| \frac{\partial \mathbf{s}_{-t}(\mathbf{x})}{\partial \mathbf{x}} \right|, \quad (4)$$

where $|\cdot|$ stands for the determinant. The infinitesimal generator for the P-F operator is given by

$$\lim_{t \rightarrow 0} \frac{[\mathbb{P}_t\varphi](\mathbf{x}) - \varphi(\mathbf{x})}{t} = -\nabla \cdot (\mathbf{F}(\mathbf{x})\varphi(\mathbf{x})) =: \mathcal{P}_{\mathbf{F}}\varphi. \quad (5)$$

These two operators are dual to each other as

$$\int_{\mathbf{X}} [\mathbb{U}_t\phi](\mathbf{x})\varphi(\mathbf{x})d\mathbf{x} = \int_{\mathbf{X}} [\mathbb{P}_t\varphi](\mathbf{x})\phi(\mathbf{x})d\mathbf{x}. \quad (6)$$

These two operators enjoy positivity and Markov properties which are used in the finite dimension approximation of these operators.

Property 1. 1) *Positivity: The P-F and Koopman operators are positive operators i.e., for any $0 \leq \varphi(\mathbf{x}) \in \mathcal{L}_\infty(\mathbf{X})$ and $0 \leq \psi(\mathbf{x}) \in \mathcal{L}_1(\mathbf{X})$, we have*

$$[\mathbb{P}_t\psi](\mathbf{x}) \geq 0, \quad [\mathbb{U}_t\varphi](\mathbf{x}) \geq 0, \quad \forall t \geq 0. \quad (7)$$

2) *Markov Property: The P-F operator satisfies Markov property i.e.,*

$$\int_{\mathbf{X}} [\mathbb{P}_t\psi](\mathbf{x})d\mathbf{x} = \int_{\mathbf{X}} \psi(\mathbf{x})d\mathbf{x}. \quad (8)$$

Definition II.3 (Almost everywhere (a.e.) stability). *The equilibrium point or an attractor set of system (1) is said to be a.e. uniform stable w.r.t. measure $\mu_0 \in \mathcal{M}(\mathbf{X})$ if*

$$\mu_0\{\mathbf{x} \in \mathbf{X} : \lim_{t \rightarrow \infty} \mathbf{s}_t(\mathbf{x}) \neq 0\} = 0, \quad (9)$$

III. PROBLEM FORMULATION FOR OFF-ROAD NAVIGATION USING TRAVERSABILITY MAP

In this section we give the definition of Traversability map as well as its mathematical description. We also provide with the choice of cost function for off-road navigation.

A. Traversability Map

In this paper, we assume that the traversability description of the terrain is captured using a positive function $b(\mathbf{x}) \in \mathcal{L}_1(\mathbf{X})$. We assume that the function $b(\mathbf{x})$ captures the information of the elevation map, terrain roughness, slope and terrain texture. Construction of such map is an active area of interest where on-board sensors on the vehicles such as vision, LIDAR, and IMU as well as drone sensory images can be used in the construction of such maps [17]–[19].

Now, let $\mu_b \in \mathcal{M}(\mathbf{X})$ be the associated traversability measure i.e., $d\mu_b(\mathbf{x}) = b(\mathbf{x})d\mathbf{x}$. For any set $A \in \mathcal{B}(\mathbf{X})$, the traversability measure of the set A is defined using $b(\mathbf{x})$ as

$$\text{Trav}(A) := \int_A b(\mathbf{x})d\mathbf{x} =: \mu_b(A). \quad (10)$$

$\text{Trav}(A)$ captures the relative degree of difficulty of traversing through the region A . In particular, if $\mu_b(A_1) < \mu_b(A_2)$ where $A_i \in \mathcal{B}(\mathbf{X})$, then the region A_2 is more difficult to traverse than region A_1 . It is easy to see that the above definition of traversability measure captures the information of binary obstacle as well. In particular, if \mathbf{X}_u is an obstacle set then it can be described using the following $b(\mathbf{x})$

$$b(\mathbf{x}) = \frac{1}{\lambda(\mathbf{X}_u)} \mathbb{1}_{\mathbf{X}_u}(\mathbf{x}) \quad (11)$$

where $\lambda(\cdot)$ is the Lebesgue measure and $\mathbb{1}_{\mathbf{X}_u}$ is the indicator function of the set \mathbf{X}_u . To describe the problem formulation for the off-road navigation, we consider the control dynamical system in the control affine form as

$$\dot{\mathbf{x}} = \mathbf{f}(\mathbf{x}) + \mathbf{g}(\mathbf{x})\mathbf{u} \quad (12)$$

where $\mathbf{x} \in \mathbf{X} \subset \mathbb{R}^n$ and $\mathbf{u} \in \mathbf{U} \subset \mathbb{R}^m$ are the states and control input respectively. The control dynamical system is assumed to model the control dynamics of the vehicle. The control-affine form of the system is not restrictive

and this will typically be the case for the robotics and vehicle dynamics application [20], [21]. The objective is to determine the control inputs $\mathbf{u}(t)$ to navigate the vehicle dynamics from some initial state \mathbf{X}_0 to some final state \mathbf{X}_T while keeping the traversability cost below some threshold, say $\bar{\gamma}$, i.e.,

$$\int_0^\infty b(\mathbf{x}(t))dt \leq \bar{\gamma} \quad (13)$$

where $\mathbf{x}(t)$ is the trajectory of the control system (17). In this paper, we are interested in asymptotic navigation problem. In the following subsection, we will discuss possible choices of cost function that are meaningful for the off-road navigation problem.

B. Choice of Cost function for Off-road Navigation

One of the obvious approach for constructing the cost function for off-road navigation is to minimize the traversability cost i.e.,

$$\min_{\mathbf{u}} \int_0^\infty b(\mathbf{x}(t))dt. \quad (14)$$

At first glance it appears that the form of cost function will incentives traversing through the region where the traversability function $b(\mathbf{x})$ takes smaller values. However, with no cost on the control input it is possible for the system trajectories to pass through the region with large value of $b(\mathbf{x})$ and hence deemed unfavorable to traverse at very high speed without negatively impacting the cost. Clearly, this kind of behavior is not tolerable. To address this problem, the cost function can be modified to ensure that occupancy in the nontraversable region is minimized as follows

$$\min_{\mathbf{u}} V_1(\mathbf{x}) = \min_{\mathbf{u}} \int_0^\infty b(\mathbf{x}(t))\|\mathbf{u}(t)\|_1 dt. \quad (15)$$

where $\|\cdot\|_1$ is the vector one norm. The above form of cost function will penalize the control input and the hence the speed of the vehicle in the nontraversable region. Another modification to the cost function can be considered as follows:

$$\min_{\mathbf{u}} V_2(\mathbf{x}) = \min_{\mathbf{u}} \int_0^\infty \alpha b(\mathbf{x}(t)) + \beta b(\mathbf{x}(t))\|\mathbf{u}(t)\|_1 dt. \quad (16)$$

where α and β are positive parameters and determine the relative weights of the traversability measure $b(\mathbf{x})$ and traversability times speed i.e, $b(\mathbf{x})|\mathbf{u}|$.

Our proposed density-based formulation relies on minimization of the cost function which is average or expected value of the above defined cost functions (31)-(16). The expected value is taken with respect to the initial measure μ_0 capturing the distribution of the initial state. Under the assumption that μ_0 is supported on the initial set \mathbf{X}_0 , we consider following cost function in our density-based formulation

$$J_k(\mu_0) = \int_{\mathbf{X}} V_k(\mathbf{x})d\mu_0(\mathbf{x}), \quad k = 1, 2 \quad (17)$$

where μ_0 is the given initial measure assumed to be absolutely continuous with density function h_0 i.e., $\frac{\partial \mu_0}{\partial \mathbf{x}} = h_0(\mathbf{x})$. Appropriate conditions on the initial measure μ_0 are necessary to ensure that the cost function is finite. We will discuss this in the main results section. Along with minimizing the cost function it is also of interest to avoid certain obstacle set, \mathbf{X}_u , and limit the control authority i.e., $|u_j| \leq L_j$. The obstacle avoidance constraints for a.e trajectories starting from the initial set \mathbf{X}_0 can be written as

$$\int_{\mathbf{X}} \mathbb{1}_{\mathbf{X}_u}(\mathbf{x}(t))d\mu_0(\mathbf{x}) = 0, \quad \forall t \geq 0.$$

where $\mathbf{x}(t)$ is the solution of system (12) starting from initial condition \mathbf{x} . With the above definition, the problem statement for the optimal off-road navigation using the traversability map can be stated as follows.

Problem 1. (Optimal off-road Navigation Problem): The optimal off-road navigation problem consists of navigation almost every system trajectories for the control system (12) starting from the initial set \mathbf{X}_0 to the target set \mathbf{X}_T while avoiding the obstacle set \mathbf{X}_u such that the following cost function is minimized and cost for traversing is kept below some threshold. Mathematically, it can be written as

$$\min_{\mathbf{u}} \int_{\mathbf{X}} \int_0^\infty \alpha b(\mathbf{x}(t)) + \beta b(\mathbf{x}(t))\|\mathbf{u}(t)\|_1 dt d\mu_0(\mathbf{x}) \quad (18a)$$

$$\text{s.t.} \quad \int_{\mathbf{X}} \mathbb{1}_{\mathbf{X}_u}(\mathbf{x}(t))d\mu_0(\mathbf{x}) = 0, \quad \forall t \geq 0 \quad (18b)$$

$$\int_{\mathbf{X}} \int_0^\infty b(\mathbf{x}(t))dt d\mu_0(\mathbf{x}) \leq \gamma \quad (18c)$$

$$|u_j| \leq L_j \quad (18d)$$

$$\dot{\mathbf{x}} = \mathbf{f}(\mathbf{x}) + \mathbf{g}(\mathbf{x})\mathbf{u}, \quad \lim_{t \rightarrow \infty} \mathbf{x}(t) \in \mathbf{X}_T \quad (18e)$$

above has to be true for almost all $\mathbf{x}(0) \in \mathbf{X}_0$. In the following section, we prove that the optimal off-road navigation problem can be written as a convex optimization problem over the density space.

IV. CONVEX FORMULATION TO OPTIMAL OFF-ROAD NAVIGATION

We consider the control affine dynamical system

$$\dot{\mathbf{x}} = \mathbf{f}(\mathbf{x}) + \mathbf{g}(\mathbf{x})\mathbf{u} \quad (19)$$

where $\mathbf{f}(\mathbf{x}) \in \mathcal{C}^1(\mathbf{X}, \mathbb{R}^n)$ and $\mathbf{g} \in \mathcal{C}^1(\mathbf{X}, \mathbb{R}^m)$. Following assumption is made on the control dynamical system and the controller for the system (19).

Assumption 1. For the optimal off-road navigation problem we assume that the optimal control input is feedback in nature i.e., $\mathbf{u} = \mathbf{k}(\mathbf{x}) \in \mathcal{C}^1(\mathbf{X})$, such that the cost function corresponding to this input is finite.

With the above assumption we can write the feedback control system in the form

$$\dot{\mathbf{x}} = \mathbf{f}(\mathbf{x}) + \mathbf{g}(\mathbf{x})\mathbf{k}(\mathbf{x}) =: \mathbf{F}_c(\mathbf{x}). \quad (20)$$

We will use the notations $\mathbf{s}_t^c(\mathbf{x})$, \mathbb{U}_t^c , and \mathbb{P}_t^c to denote the solution, the Koopman operator, and the P-F operator for the closed loop system (20). The first results of this section allows us to write the obstacle avoidance constraints (18b) in the integral form.

Lemma 1. *For the dynamical system (20), if*

$$\int_0^\infty \int_{\mathbf{X}} \mathbb{1}_{\mathbf{X}_u}(\mathbf{s}_t^c(\mathbf{x})) d\mu_0(\mathbf{x}) dt = 0 \quad (21)$$

then

$$\int_{\mathbf{X}} \mathbb{1}_{\mathbf{X}_u}(\mathbf{s}_t^c(\mathbf{x})) h_0(\mathbf{x}) d\mathbf{x} = 0, \quad \forall t \geq 0, \quad (22)$$

i.e., the amount of time system trajectories spend in the region \mathbf{X}_u starting from the positive measure set of initial condition corresponding to the initial set, \mathbf{X}_0 , with density $h_0(\mathbf{x})$ is equal to zero.

Proof. Proof by contradiction. Assume (22) is not true, i.e., there exists some time t_0 for which

$$\int_{\mathbf{X}} \mathbb{1}_{\mathbf{X}_u}(\mathbf{s}_{t_0}^c(\mathbf{x})) h_0(\mathbf{x}) d\mathbf{x} = \int_{\mathbf{X}_1} [\mathbb{U}_{t_0}^c \mathbb{1}_{\mathbf{X}_u}](\mathbf{x}) h_0(\mathbf{x}) d\mathbf{x} > 0$$

Then using the continuity property of the Koopman semi-group, we know there exists a Δ such that

$$\int_{t_0}^{t_0+\Delta} \int_{\mathbf{X}} [\mathbb{U}_{t_0}^c \mathbb{1}_{\mathbf{X}_u}](\mathbf{x}) h_0(\mathbf{x}) d\mathbf{x} dt > 0.$$

We have

$$0 < \int_{t_0}^{t_0+\Delta} \int_{\mathbf{X}} [\mathbb{U}_{t_0}^c \mathbb{1}_{\mathbf{X}_u}](\mathbf{x}) h_0(\mathbf{x}) d\mathbf{x} dt \leq \int_0^\infty \int_{\mathbf{X}} [\mathbb{U}_{t_0}^c \mathbb{1}_{\mathbf{X}_u}](\mathbf{x}) h_0(\mathbf{x}) d\mathbf{x} dt = 0 \quad (23)$$

□

Remark. *Following the results of Lemma 1, we can replace the the obstacle avoidance constraints (18b) as*

$$\int_0^\infty \int_{\mathbf{X}} \mathbb{1}_{\mathbf{X}_u}(\mathbf{s}_t^c(\mathbf{x})) d\mu_0(\mathbf{x}) dt = 0 \quad (24)$$

Remark. *In the rest of the paper, we will use notation $\mathbf{X}_1 = \mathbf{X} \setminus \mathcal{N}_\epsilon$, where \mathcal{N}_ϵ is the ϵ neighborhood of the target set. With no loss of generality we can assume that the target set \mathbf{X}_T is locally stable with domain of attraction containing \mathcal{N}_ϵ .*

We are now ready to state the main results of this paper.

Theorem 2. *Under Assumption 1, the optimal off-road navigation problem can be written as following convex optimization problem in term of optimization variable $\rho \in$*

$\mathcal{L}_1(\mathbf{X}_1) \cap \mathcal{C}^1(\mathbf{X}_1, \mathbb{R}_{\geq 0})$ and $\bar{\rho} \in \mathcal{C}^1(\mathbf{X}_1, \mathbb{R})$.

$$J^*(\mu) = \inf_{\rho, \bar{\rho}} \int_{\mathbf{X}_1} \alpha b(\mathbf{x}) \rho(\mathbf{x}) + \beta b(\mathbf{x}) \|\bar{\rho}(\mathbf{x})\|_1 d\mathbf{x} \quad (25a)$$

$$\text{s.t.} \quad \int_{\mathbf{X}_1} \mathbb{1}_{\mathbf{X}_u}(\mathbf{x}) \rho(\mathbf{x}) d\mathbf{x} = 0 \quad (25b)$$

$$\int_{\mathbf{X}_1} b(\mathbf{x}) \rho(\mathbf{x}) d\mathbf{x} \leq \gamma \quad (25c)$$

$$|\bar{\rho}_j(\mathbf{x})| \leq L_j \rho(\mathbf{x}) \quad (25d)$$

$$\nabla \cdot (\mathbf{f}\rho + \mathbf{g}\bar{\rho}) = h_0, \quad \text{a.e. } \mathbf{x} \in \mathbf{X}_1 \quad (25e)$$

The optimal feedback control input is recovered from the solution of the above optimization problem as

$$k^*(\mathbf{x}) = \frac{\bar{\rho}^*(\mathbf{x})}{\rho^*(\mathbf{x})} \quad (26)$$

where $(\rho^*, \bar{\rho}^*)$ are the solution of (25).

Proof. Following Assumption 1, we write the feedback control system

$$\dot{\mathbf{x}} = \mathbf{f}(\mathbf{x}) + \mathbf{g}(\mathbf{x})\mathbf{k}(\mathbf{x}). \quad (27)$$

Let \mathbb{P}_t^c and \mathbb{U}_t^c be P-F and Koopman operator for the feedback control system (27). Now we use the fact that $d\mu_0 = h_0(\mathbf{x})d\mathbf{x}$, and the definition of Koopman operator to write the cost function (18a) as

$$\begin{aligned} J(\mu_0) &= \int_{\mathbf{X}_1} \int_0^\infty [\mathbb{U}_t^c(\alpha b + \beta b\|\mathbf{k}\|_1)](\mathbf{x}) dt h_0(\mathbf{x}) d\mathbf{x} \\ &= \int_{\mathbf{X}_1} \int_0^\infty (\alpha b + \beta b\|\mathbf{k}\|_1)(\mathbf{s}_t^c(\mathbf{x})) dt h_0(\mathbf{x}) d\mathbf{x} \end{aligned}$$

Performing change of variable $\mathbf{y} = \mathbf{s}_t^c(\mathbf{x})$ or $\mathbf{x} = \mathbf{s}_{-t}^c(\mathbf{y})$ and using the definition of P-F operator we can write the above as

$$\begin{aligned} J(\mu_0) &= \int_{\mathbf{X}_1} \int_0^\infty (\alpha b + \beta b\|\mathbf{k}\|_1)(\mathbf{x}) [\mathbb{P}_t^c h_0] dt d\mathbf{x} \\ &= \int_{\mathbf{X}_1} (\alpha b + \beta b\|\mathbf{k}\|_1)(\mathbf{x}) \rho(\mathbf{x}) d\mathbf{x} \end{aligned} \quad (28)$$

where

$$\rho(\mathbf{x}) := \int_0^\infty [\mathbb{P}_t^c h_0](\mathbf{x}) dt. \quad (29)$$

Since the cost function is assumed to be finite (Assumption 1), the $\rho(\mathbf{x})$ is well-defined for a.e. \mathbf{x} and is an integrable function. From the definition of the P-F operator and the assumption made on function h_0 it follows that the function $[\mathbb{P}_t^c h_0](\mathbf{x})$ is uniformly continuous function of time. Hence using Barbalat Lemma [22, pg. 269] we have

$$\lim_{t \rightarrow \infty} [\mathbb{P}_t^c h_0](\mathbf{x}) = 0, \quad (30)$$

for a.e. \mathbf{x} . Furthermore, since the P-F operator is a positive operator (Property 1) and $h_0(\mathbf{x}) \geq 0$, we have $\rho(\mathbf{x}) \geq 0$. Hence (31) can be written as

$$J(\mu_0) = \int_{\mathbf{X}_1} \alpha b(\mathbf{x}) \rho(\mathbf{x}) + \beta b(\mathbf{x}) \|\bar{\rho}(\mathbf{x})\|_1 d\mathbf{x} \quad (31)$$

where $\bar{\rho}(\mathbf{x}) := \rho(\mathbf{x})\mathbf{k}(\mathbf{x})$. This shows that the cost function in (18) can be written in the form (25). We next discuss the constraints. Following the results of Lemma 1, we know that (21) implies (22). Hence, the obstacle avoidance constraints (18c) is implied by

$$\int_0^\infty \int_{\mathbf{X}} \mathbb{1}_{\mathbf{X}_u}(\mathbf{s}_t^c(\mathbf{x})) d\mu_0(\mathbf{x}) dt = 0 \quad (32)$$

Again performing change of variables $\mathbf{y} = \mathbf{s}_t^c(\mathbf{x})$ and using the definition of P-F operator, (32) can be written as

$$\int_{\mathbf{X}_1} \mathbb{1}_{\mathbf{X}_u}(\mathbf{x}) \rho(\mathbf{x}) d\mathbf{x} = 0$$

with $\rho(\mathbf{x})$ as defined in (29). Similarly, it follows that (18d) can be written as

$$\int_{\mathbf{X}_1} b(\mathbf{x}) \rho(\mathbf{x}) d\mathbf{x} \leq \gamma.$$

The control constraints $|u_j| \leq L_j$ for $j = 1, \dots, m$ can be written as $|\bar{\rho}_j(\mathbf{x})| \leq L_j \rho(\mathbf{x})$ follows from the fact that $\mathbf{u} = \mathbf{k}(\mathbf{x}) = \bar{\rho}(\mathbf{x})/\rho(\mathbf{x})$ and $\rho(\mathbf{x})$ is positive. We next show that the $\rho(\mathbf{x})$ as defined in (29) satisfies the constraints (25e). Substituting (29) in the constraint of (25e), we obtain

$$\begin{aligned} \nabla \cdot (\mathbf{f}_c(\mathbf{x}) \rho(\mathbf{x})) &= \int_0^\infty \nabla \cdot (\mathbf{f}_c(\mathbf{x}) [\mathbb{P}_t^c h_0](\mathbf{x})) dt \\ &= \int_0^\infty -\frac{d}{dt} [\mathbb{P}_t^c h_0](\mathbf{x}) dt = -[\mathbb{P}_t^c h_0](\mathbf{x}) \Big|_{t=0}^\infty = h_0(\mathbf{x}), \end{aligned} \quad (33)$$

where, $\mathbf{f}_c(\mathbf{x}) := \mathbf{f}(\mathbf{x}) + \mathbf{g}(\mathbf{x})\mathbf{k}(\mathbf{x})$. In deriving (33) we have used the infinitesimal generator property of P-F operator Eq. (5) and the fact that $\lim_{t \rightarrow \infty} [\mathbb{P}_t^c h_0](\mathbf{x}) = 0$ following (30). We next show that the target set \mathbf{X}_T is a.e. stable w.r.t measure μ_0 supported on the initial set \mathbf{X}_0 . Consider the set S_ℓ

$$S_\ell = \{\mathbf{x} \in \mathbf{X}_1 : \mathbf{s}_t^c(\mathbf{x}) \in \mathbf{X}_1, \text{ for some } t > \ell\}$$

and let

$$S = \bigcap_{\ell=1}^\infty S_\ell$$

The set S contains points some of whose limit points lie in \mathbf{X}_1 and for almost every stability of the target set we need to show that $\mu_0(S) = 0$. From the construction of the set S , it follows that $\mathbf{s}_t^c(S) = S$, where $\mathbf{s}_t^c(S) = \{\mathbf{s}_t^c(\mathbf{x}) : \mathbf{x} \in S\}$.

$$\begin{aligned} \mu_0(S) &= \int_{\mathbf{X}_1} \lambda_S(\mathbf{x}) h_0(\mathbf{x}) d\mathbf{x} = \int_{\mathbf{X}_1} \lambda_S(\mathbf{s}_t^c(\mathbf{x})) h_0(\mathbf{x}) d\mathbf{x} \\ &= \int_{\mathbf{X}_1} \lambda_S(\mathbf{x}) [\mathbb{P}_t h_0](\mathbf{x}) d\mathbf{x} \end{aligned} \quad (34)$$

where we have use the fact that $\mathbf{x} \in S$ iff $\mathbf{s}_t^c(\mathbf{x}) \in S$. Since the above is true for all $t \geq 0$, we obtain using dominated convergence theorem

$$\mu_0(S) = \lim_{t \rightarrow \infty} \int_{\mathbf{X}_1} [\mathbb{P}_t h_0](\mathbf{x}) d\mathbf{x} = \int_{\mathbf{X}_1} \lim_{t \rightarrow \infty} [\mathbb{P}_t h_0](\mathbf{x}) d\mathbf{x} = 0$$

□

Other constraints on the state and control input that can be written convexly in terms of the optimization variables ρ and $\bar{\rho}$ can be incorporated in the framework. As we show in the simulation section one of such constraints is the curvature constraints. For example, consider a Dubin's car model

$$\dot{x}_1 = u_1 \cos \theta, \quad \dot{x}_2 = u_1 \sin \theta, \quad \dot{\theta} = u_2.$$

Aside from the kinematic constraints imposed by nonholonomy, most often the additional constraint that the radius of curvature of the paths of the vehicle are lower bounded must be considered [23]. The curvature constraints itself will be function of the terrain properties. The curvature constraints makes the kinematic model of Dubin's car more close to reality. The curvature constraints are captured as follows.

$$\frac{|u_2|}{|u_1|} \leq \frac{1}{C} \quad (35)$$

where u_2 is the angular velocity of the Dubin's car model. The constraint in (35) makes sure that control design are realistic and that angular velocity of the kinematic model is bounded. The (35) can be easily added to the optimization problem of theorem 2 convexly as follows. Following the general formulation specialize for two input system, we can write $u_1 = \frac{\bar{\rho}_1}{\rho}$ and $u_2 = \frac{\bar{\rho}_2}{\rho}$, hence

$$\frac{|u_2|}{|u_1|} \leq \frac{1}{C} \implies C|\bar{\rho}_2| - |\bar{\rho}_1| \leq 0 \quad (36)$$

which is linear and hence convex in $\bar{\rho}_1$ and $\bar{\rho}_2$.

V. COMPUTATIONAL FRAMEWORK

In this section, we provide with a new data driven approximation, namely NSDMD*, which is a modification of Naturally structured dynamic mode decomposition (NSDMD) [24]. Then we will formulate our problem statement with the given computational framework.

A. Data-Driven Approximation: NSDMD*

Naturally structured dynamic mode decomposition (NSDMD) is a modification of Extended Dynamic Mode Decomposition (EDMD) algorithm [25], one of the popular algorithms used for the data-driven approximation of the Koopman operator. The modifications in NSDMD were introduced to incorporate the natural properties of these operators namely the positivity and the Markov properties. However, these modifications are computationally expensive. Our proposed transfer operator theoretic framework for the control design relies on the positivity and Markov properties of these operators. In our proposed modification of the NSDMD algorithm we gain numerical efficiency at the expense of preserving these properties approximately. We call this modified algorithm as NSDMD*. For the continuous-time dynamical system (1), consider snapshots of data set obtained as time-series data from single or multiple trajectories.

$$\mathcal{X} = [\mathbf{x}_1, \mathbf{x}_2, \dots, \mathbf{x}_M], \quad \mathcal{Y} = [\mathbf{y}_1, \mathbf{y}_2, \dots, \mathbf{y}_M], \quad (37)$$

where $\mathbf{x}_i \in \mathbf{X}$ and $\mathbf{y}_i \in \mathbf{X}$. The pair of data sets are assumed to be two consecutive snapshots i.e., $\mathbf{y}_i = \mathbf{s}_{\Delta t}(\mathbf{x}_i)$.

In our proposed data-driven computation, the pair of two consecutive snapshots are obtained using system with no control input ($\mathbf{s}_{\Delta t}^0(\mathbf{x}_i)$) and with the step input ($\mathbf{s}_{\Delta t}^1(\mathbf{x}_i)$). Let $\Psi = [\psi_1, \dots, \psi_N]^\top$ be the choice of basis functions. The EDMD algorithm computes the finite-dimensional approximation of the Koopman operator (\mathbf{U}) as the result of the following least square problem.

$$\min_{\mathbf{U}} \|\mathbf{G}\mathbf{U} - \mathbf{A}\|_F, \quad (38)$$

where,

$$\mathbf{G} = \frac{1}{M} \sum_{m=1}^M \Psi(\mathbf{x}_m) \Psi(\mathbf{x}_m)^\top, \quad (39)$$

$$\mathbf{A} = \frac{1}{M} \sum_{m=1}^M \Psi(\mathbf{x}_m) \Psi(\mathbf{y}_m)^\top, \quad (40)$$

with $\mathbf{U}, \mathbf{G}, \mathbf{A} \in \mathbb{R}^{N \times N}$, $\|\cdot\|_F$ stands for Frobenius norm. The above least square problem admits an analytical solution

$$\mathbf{U}^* = \mathbf{G}^\dagger \mathbf{A}. \quad (41)$$

Convergence results for EDMD algorithms in the limit as the number of data points and basis functions go to infinity are provided in [26], [27]. In this paper, we work with Gaussian Radial Basis Function (RBF) for the finite-dimensional approximation of the linear operators, which are positive basis. Under the assumption that the basis functions are positive our proposed NSDMD* obtains $\hat{\mathbf{U}}$ from \mathbf{U}^* using row normalization i.e., the entries of the matrix $\hat{\mathbf{U}}$ are obtained as follows.

$$[\hat{\mathbf{U}}]_{ij} = \frac{[\mathbf{U}^*]_{ij}}{\sum_j [\mathbf{U}^*]_{ij}} \quad (42)$$

The P-F matrix is then obtained as $\hat{\mathbf{P}} = \hat{\mathbf{U}}^\top$. The generator of P-F operator are obtained as

$$\mathcal{P}_F \approx \frac{\hat{\mathbf{P}} - \mathbf{I}}{\Delta t} =: \mathbf{M}. \quad (43)$$

Note that in the above construction, we did not strictly enforce the positivity property on the linear operators. However, the numerical evidence suggest that the entries of the matrix, \mathbf{U}^* obtained using the EDMD algorithm with positive basis function are predominantly positive.

B. Problem Statement Computational Framework

This section discusses about finite dimensional approximation of the infinite dimensional optimal navigation problem (25a)-(25c). We use the approximation of the generator for the vector field \mathbf{f} and \mathbf{g} . The generator approximation of the two vector fields are given as follows

$$\mathcal{P}_f \approx \mathbf{M}_0, \quad \mathcal{P}_g \approx \mathbf{M}_1 \quad (44)$$

The generator approximation of \mathcal{P}_f starts with obtaining open-loop time series data $\{\mathbf{x}_k^0\} = \{\mathbf{x}_0^0, \mathbf{x}_1^0, \dots, \mathbf{x}_M^0\}$ by substituting $\mathbf{u} = 0$ in (12). Similarly, the approximation of \mathcal{P}_g is obtained by getting $\{\mathbf{x}_k^i\} = \{\mathbf{x}_0^i, \mathbf{x}_1^i, \dots, \mathbf{x}_M^i\}$ from substituting $\mathbf{u} = \mathbf{u}_i$ in (12) where \mathbf{u}_i is a column vector consisting of all zeros except at i^{th} position where the

element value is 1. Then we calculate the matrices $\hat{\mathbf{U}}^0$ and $\hat{\mathbf{U}}^i$ by utilizing (38)-(42). The P-F matrix is then obtained as $\hat{\mathbf{P}}^0 = \hat{\mathbf{U}}^{0\top}$ and $\hat{\mathbf{P}}^i = \hat{\mathbf{U}}^{i\top}$. Then we calculate \mathbf{M}_0 and \mathbf{M}_i as follows:

$$\mathcal{P}_f \approx \frac{\hat{\mathbf{P}}^0 - \mathbf{I}}{\Delta t} =: \mathbf{M}_0, \quad \mathcal{P}_{f+g_i} \approx \frac{\hat{\mathbf{P}}^i - \mathbf{I}}{\Delta t} \quad (45)$$

$$\text{and } \mathcal{P}_{g_i} = \mathcal{P}_{f+g_i} - \mathcal{P}_f =: \mathbf{M}_i \quad (46)$$

NSDMD* algorithm outlined in Section V-A is used to approximate with $\Psi(\mathbf{x}) = [\psi_1(\mathbf{x}), \psi_2(\mathbf{x}), \dots, \psi_N(\mathbf{x})]^\top$ as the basis functions. Let $\bar{\rho}(\mathbf{x}) = [\bar{\rho}_1(\mathbf{x}), \dots, \bar{\rho}_m(\mathbf{x})]^\top$ and $\Gamma(\mathbf{x}) = [\Gamma_1(\mathbf{x}), \dots, \Gamma_m(\mathbf{x})]^\top$. Now let us express the following terms as combinations of basis functions

$$h_0(\mathbf{x}) = \Psi^\top \mathbf{m}, \quad \rho(\mathbf{x}) = \Psi^\top \mathbf{v}, \quad \bar{\rho}_j(\mathbf{x}) = \Psi^\top \mathbf{w}_j, \quad \Gamma_j(\mathbf{x}) = \Psi^\top \mathbf{r}_j. \quad (47)$$

where $|\bar{\rho}_j(\mathbf{x})| < \Gamma_j(\mathbf{x})$. Minimizing $\Gamma_j(\mathbf{x})$ will indirectly minimize $|\bar{\rho}_j(\mathbf{x})|$. Therefore we replace $\|\bar{\rho}(\mathbf{x})\|_1$ by $\sum_j \Gamma_j(\mathbf{x})$ in (25a) and then perform the following finite-dimensional approximation.

$$\inf_{\rho, \bar{\rho}} \int_{\mathbf{X}_1} \left[\alpha b(\mathbf{x}) \rho(\mathbf{x}) + \beta b(\mathbf{x}) \sum_j \Gamma_j(\mathbf{x}) \right] d\mathbf{x} \approx \min_{\mathbf{r}_j, \mathbf{w}_j, \mathbf{v}} \mathbf{D}_1^\top \mathbf{v} + \mathbf{D}_2^\top \sum_j \mathbf{r}_j \quad (48a)$$

$$\text{s.t. } \mathbf{r}_j - \mathbf{w}_j > \mathbf{0} \quad (48b)$$

$$\mathbf{r}_j + \mathbf{w}_j > \mathbf{0} \quad (48c)$$

where $\mathbf{D}_1 = \int_{\mathbf{X}_1} \alpha b(\mathbf{x}) \Psi(\mathbf{x}) d\mathbf{x}$, $\mathbf{D}_2 = \int_{\mathbf{X}_1} \beta b(\mathbf{x}) \Psi(\mathbf{x}) d\mathbf{x}$ and $\mathbf{0}$ is a zero vector.

Similarly, we can write

$$\int_{\mathbf{X}_1} \mathbb{1}_{\mathbf{X}_u}(\mathbf{x}) \rho(\mathbf{x}) d\mathbf{x} \approx \left[\int_{\mathbf{X}_1} \mathbb{1}_{\mathbf{X}_u}(\mathbf{x}) \Psi(\mathbf{x}) d\mathbf{x} \right] \mathbf{v} = \mathbf{d}_1^\top \mathbf{v} \quad (49)$$

where $\mathbf{d}_1 := \int_{\mathbf{X}_1} \mathbb{1}_{\mathbf{X}_u}(\mathbf{x}) \Psi(\mathbf{x}) d\mathbf{x}$.

Similarly,

$$\int_{\mathbf{X}_1} b(\mathbf{x}) \rho(\mathbf{x}) d\mathbf{x} \approx \left[\int_{\mathbf{X}_1} b(\mathbf{x}) \Psi^\top(\mathbf{x}) d\mathbf{x} \right] \mathbf{v} = \mathbf{d}_2^\top \mathbf{v} \quad (50)$$

where $\mathbf{d}_2 := \int_{\mathbf{X}_1} b(\mathbf{x}) \Psi(\mathbf{x}) d\mathbf{x}$.

Assumption 2. We consider all the basis functions to be positive and linearly independent.

Remark. We use Gaussian Radial Basis Functions (RBF) in this paper to obtain all the simulation results i.e., $\psi_k(\mathbf{x}) = \exp^{-\frac{\|\mathbf{x} - \mathbf{c}_k\|^2}{2\sigma^2}}$ where \mathbf{c}_k is the center of the k^{th} Gaussian RBF.

Therefore the ONP in Theorem 2 can be written as

$$\begin{aligned}
& \min_{\mathbf{r}_j, \mathbf{w}_j, \mathbf{v}} \mathbf{D}_1^\top \mathbf{v} + \mathbf{D}_2^\top \sum_j \mathbf{r}_j \\
& \text{s.t.} \quad \mathbf{r}_j - \mathbf{w}_j > \mathbf{0} \\
& \quad \mathbf{r}_j + \mathbf{w}_j > \mathbf{0} \\
& \quad -\mathbf{M}_0 \mathbf{v} - \sum_j \mathbf{M}_j \mathbf{w}_j = \mathbf{m} \\
& \quad \mathbf{d}_1 \mathbf{v} = 0 \\
& \quad \mathbf{d}_2 \mathbf{v} \leq \gamma \\
& \quad |\mathbf{w}_j| \leq L_j \mathbf{v}
\end{aligned}$$

VI. SIMULATION RESULTS

The simulation results in this paper are obtained using Gaussian RBF. The centers of the RBF are chosen to be uniformly distributed in the state space at a distance of d . The standard deviation σ for the Gaussian RBF is chosen to be between $d \leq 3\sigma \leq 1.5d$. All the simulation results are performed using MATLAB on a desktop computer with 64 GB RAM. The linear approximation of the underlying system dynamics are computed using the data of the UGV. In this paper, we use the dubin's car model dynamics to present the results. CVX toolbox is used for solving optimization problem.

Example. The simulation results are obtained using Dubin's car dynamics

$$\dot{x}_1 = u_1 \cos \theta, \quad \dot{x}_2 = u_1 \sin \theta, \quad \dot{\theta} = u_2 \quad (51)$$

We consider two different configuration of initial and terminal set labeled as $\mathbf{X}_{01}, \mathbf{X}_{02}$ and $\mathbf{X}_{T1}, \mathbf{X}_{T2}$. These sets are described as follows.

- $\mathbf{X} \triangleq \{\mathbf{x} \in \mathbb{R}^3 : -3 \leq x_1 \leq 9, -3 \leq x_2 \leq 9, -3 \leq x_3 \leq 3\}$
- $\mathbf{X}_{01} \triangleq \{\mathbf{x} \in \mathbb{R}^2 : 1 - (x_1 - 5.5)^2 - (x_2 - 7.5)^2 \geq 0\}$
- $\mathbf{X}_{02} \triangleq \{\mathbf{x} \in \mathbb{R}^2 : 1 - (x_1 + 0.5)^2 - (x_2 + 1.5)^2 \geq 0\}$
- $\mathbf{X}_{T1} \triangleq \{\mathbf{x} \in \mathbb{R}^2 : 1 - x_1^2 - x_2^2 \geq 0\}$
- $\mathbf{X}_{T2} \triangleq \{\mathbf{x} \in \mathbb{R}^2 : 1 - (x_1 - 8)^2 - (x_2 - 3)^2 \geq 0\}$
- $\mathbf{X}_u \triangleq \{\mathbf{x} \in \mathbb{R}^2 : 1 - (x_1 - 3)^2 - (x_2 - 4)^2 \geq 0\}$

The linear operators are approximated using 2500 RBF and the time-step of discretization $\Delta t = 0.01$. We have obtained the results for two different traversability maps labeled by $b_1(\mathbf{x})$ and $b_2(\mathbf{x})$. In Fig. 1, we show the plot for initial conditions centered around (6.4, 8.5) in initial set \mathbf{X}_{01} navigating successfully to terminal set \mathbf{X}_{T1} with traversability map given by $b_1(\mathbf{x})$. We notice that the trajectories navigate through a region where the traversability map takes smaller values. Similarly, Fig. 2 shows the simulation results for optimal navigation from the initial set \mathbf{X}_{02} to terminal set \mathbf{X}_{T2} with traversability map given by $b_2(\mathbf{x})$. The control plots for the trajectories given in Fig. 1 are displayed in Fig. 3. The control limits are set to be ± 3 and are seen to be met by the control.

The optimal navigation problem given in (25a) - (25d) can also be utilized to avoid any particular predetermined region such as enemy camp, lake or pits. We show the optimal navigation plots without and with such a hard obstacle set

\mathbf{X}_u in Fig. 4a and Fig. 4b respectively. The corresponding density plots ($\rho(\mathbf{x})$) for the trajectories with and without hard obstacles are shown in Fig. 5a and Fig. 5b.

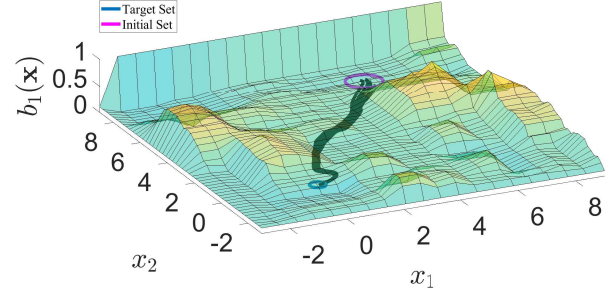


Fig. 1: Optimal navigation with initial points centered around (6.4, 8.5) in initial set \mathbf{X}_{01} to terminal set \mathbf{X}_{T1} with traversability map given by $b_1(\mathbf{x})$.

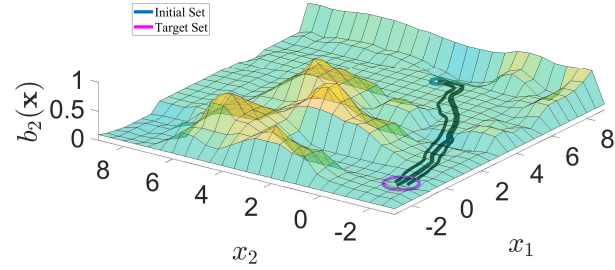


Fig. 2: Optimal navigation with initial points centered around (-0.5, -1.5) in initial set \mathbf{X}_{02} to terminal set \mathbf{X}_{T2} with traversability map given by $b_2(\mathbf{x})$.

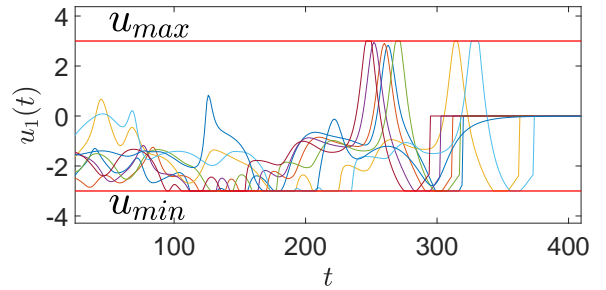
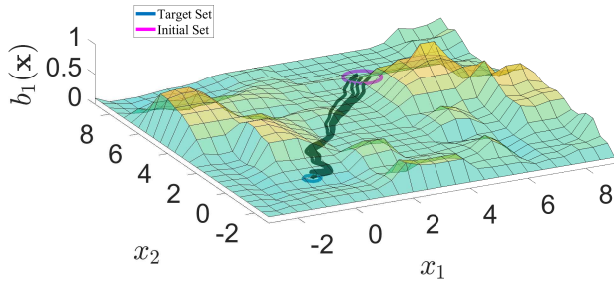


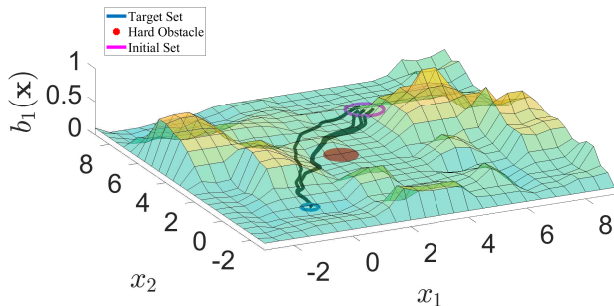
Fig. 3: Optimal control plots for u_1 corresponding to different initial conditions with configuration of initial and final sets as in Fig. 1.

VII. CONCLUSION

The problem of navigation on off-road terrain is considered. We use traversability measure to describe the relative degree of difficulty of navigation. A convex formulation for the optimal navigation problem is constructed using the traversability information of the terrain. The convex formulation leads to an infinite-dimensional convex optimization



(a) Optimal navigation with initial points centered around (5.5, 7.5) in initial set \mathbf{X}_{01} to terminal set \mathbf{X}_{T1} with traversability map given by $b_1(\mathbf{x})$.



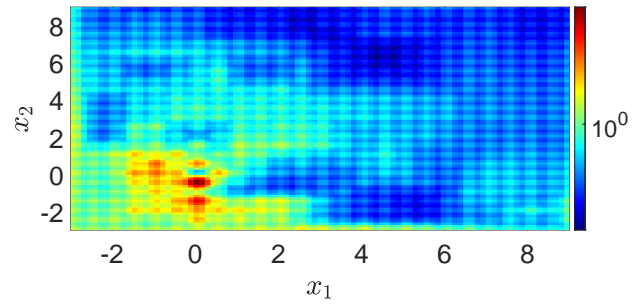
(b) Optimal navigation with initial points centered around (5.5, 7.5) in initial set \mathbf{X}_{01} to terminal set \mathbf{X}_{T1} with traversability map given by $b_1(\mathbf{x})$. The traversability map includes hard obstacle centered around (3, 4).

Fig. 4: Navigation with and without hard obstacles.

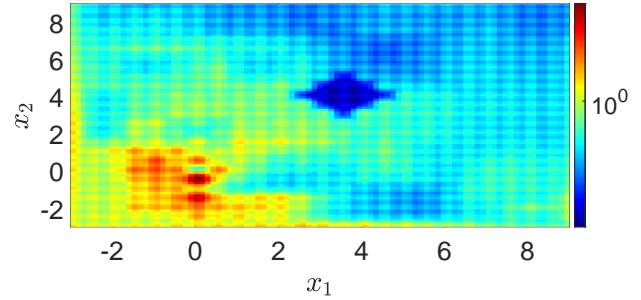
problem for navigation. Furthermore, we utilize the data-driven approximation of the linear P-F operator for the finite-dimensional approximation of the optimization problem. Finally, simulation results are showcased to show the validity of the proposed method. Future research efforts will incorporate the uncertainty arising from vehicle dynamics and vehicle-terrain interaction in the framework.

REFERENCES

- [1] M. W. Hirsch, S. Smale, and R. L. Devaney, *Differential equations, dynamical systems, and an introduction to chaos*. Academic press, 2012.
- [2] D. E. Koditschek and E. Rimon, “Robot navigation functions on manifolds with boundary,” *Advances in applied mathematics*, vol. 11, no. 4, pp. 412–442, 1990.
- [3] S. Mentasti and M. Matteucci, “Multi-layer occupancy grid mapping for autonomous vehicles navigation,” in *2019 AEIT International Conference of Electrical and Electronic Technologies for Automotive (AEIT AUTOMOTIVE)*. IEEE, 2019, pp. 1–6.
- [4] T. Overbye and S. Saripalli, “Fast local planning and mapping in unknown off-road terrain,” in *2020 IEEE International Conference on Robotics and Automation (ICRA)*. IEEE, 2020, pp. 5912–5918.
- [5] B. Gao, A. Xu, Y. Pan, X. Zhao, W. Yao, and H. Zhao, “Off-road drivable area extraction using 3d lidar data,” in *2019 IEEE Intelligent Vehicles Symposium (IV)*. IEEE, 2019, pp. 1505–1511.
- [6] Y. Yang, D. Tang, D. Wang, W. Song, J. Wang, and M. Fu, “Multi-camera visual slam for off-road navigation,” *Robotics and Autonomous Systems*, vol. 128, p. 103505, 2020.
- [7] M. Bajracharya, A. Howard, L. H. Matthies, B. Tang, and M. Turmon, “Autonomous off-road navigation with end-to-end learning for the lagr program,” *Journal of Field Robotics*, vol. 26, no. 1, pp. 3–25, 2009.



(a) Density plots for the trajectories shown in Fig. 4a.



(b) Density plots for the trajectories shown in Fig. 4b.

Fig. 5: Density plots for terrain navigation with (5b) and without (5a) hard obstacles.

- [8] A. Hussein, P. Marín-Plaza, D. Martín, A. de la Escalera, and J. M. Armingol, “Autonomous off-road navigation using stereo-vision and laser-rangefinder fusion for outdoor obstacles detection,” in *2016 IEEE Intelligent Vehicles Symposium (IV)*. IEEE, 2016, pp. 104–109.
- [9] T. Overbye and S. Saripalli, “G-vom: A gpu accelerated voxel off-road mapping system,” *arXiv preprint arXiv:2109.13176*, 2021.
- [10] D. Hoeller, L. Wellhausen, F. Farshidian, and M. Hutter, “Learning a state representation and navigation in cluttered and dynamic environments,” *IEEE Robotics and Automation Letters*, vol. 6, no. 3, pp. 5081–5088, 2021.
- [11] B. Huang and U. Vaidya, “A convex approach to data-driven optimal control via perron-frobenius and koopman operators,” *arXiv preprint arXiv:2010.01742*; (accepted for publication in *IEEE Transactions on Automatic Control*), 2020.
- [12] H. Yu, J. Moyalan, U. Vaidya, and Y. Chen, “Data-driven optimal control of nonlinear dynamics under safety constraints,” *IEEE Control Systems Letters*, 2022.
- [13] U. Vaidya, “Optimal motion planning using navigation measure,” *International Journal of Control*, vol. 91, no. 5, pp. 989–998, 2018.
- [14] J. Moyalan, H. Choi, Y. Chen, and U. Vaidya, “Sum of squares based convex approach for optimal control synthesis,” in *2021 29th Mediterranean Conference on Control and Automation (MED)*. IEEE, 2021, pp. 1270–1275.
- [15] J. Moyalan, Y. Chen, and U. Vaidya, “Navigation with probabilistic safety constraints: Convex formulation,” in *accepted to be presented at American Control Conference 2022*. IEEE, 2022.
- [16] A. Lasota and M. C. Mackey, *Chaos, fractals, and noise: stochastic aspects of dynamics*. Springer Science & Business Media, 1998, vol. 97.
- [17] H. Huang, A. V. Savkin, and C. Huang, “Decentralized autonomous navigation of a uav network for road traffic monitoring,” *IEEE Transactions on Aerospace and Electronic Systems*, vol. 57, no. 4, pp. 2558–2564, 2021.
- [18] C. Armbrust, T. Braun, T. Föhst, M. Proetzsch, A. Renner, B.-H. Schäfer, and K. Berns, “Ravon: The robust autonomous vehicle for off-road navigation,” in *Using Robots in Hazardous Environments*. Elsevier, 2011, pp. 353–396.
- [19] N. Bagheri, “Development of a high-resolution aerial remote-sensing

- system for precision agriculture,” *International journal of remote sensing*, vol. 38, no. 8-10, pp. 2053–2065, 2017.
- [20] X. Xiao, J. Biswas, and P. Stone, “Learning inverse kinodynamics for accurate high-speed off-road navigation on unstructured terrain,” *IEEE Robotics and Automation Letters*, vol. 6, no. 3, pp. 6054–6060, 2021.
- [21] J. M. Gregory, G. Warnell, J. Fink, and S. K. Gupta, “Improving trajectory tracking accuracy for faster and safer autonomous navigation of ground vehicles in off-road settings,” in *2021 IEEE International Symposium on Safety, Security, and Rescue Robotics (SSRR)*. IEEE, 2021, pp. 204–209.
- [22] I. Barbalat, “Systemes d’équations différentielles d’oscillations non linéaires,” *Rev. Math. Pures Appl*, vol. 4, no. 2, pp. 267–270, 1959.
- [23] A. Balluchi, A. Bicchi, A. Balestrino, and G. Casalino, “Path tracking control for dubin’s cars,” in *Proceedings of IEEE International Conference on Robotics and Automation*, vol. 4. IEEE, 1996, pp. 3123–3128.
- [24] B. Huang and U. Vaidya, “Data-driven approximation of transfer operators: Naturally structured dynamic mode decomposition,” in *2018 Annual American Control Conference (ACC)*. IEEE, 2018, pp. 5659–5664.
- [25] M. O. Williams, I. G. Kevrekidis, and C. W. Rowley, “A data-driven approximation of the koopman operator: Extending dynamic mode decomposition,” *Journal of Nonlinear Science*, vol. 25, no. 6, pp. 1307–1346, 2015.
- [26] M. Korda and I. Mezić, “On convergence of extended dynamic mode decomposition to the koopman operator,” *Journal of Nonlinear Science*, vol. 28, no. 2, pp. 687–710, 2018.
- [27] S. Klus, I. Schuster, and K. Muandet, “Eigendecompositions of transfer operators in reproducing kernel hilbert spaces,” *Journal of Nonlinear Science*, vol. 30, no. 1, pp. 283–315, 2020.